
Dynamics and Stability of Magnetic-Air Hybrid Quasi-Zero Stiffness Vibration Isolation System

Youliang Jiang

*School of Mechanical and Electronic Engineering, Wuhan University of Technology, Wuhan 430070, China.
Hubei Provincial Engineering Technology Research Center for Magnetic Suspension, Wuhan 430070, China.*

Chunsheng Song

*School of Mechanical and Electronic Engineering, Wuhan University of Technology, Wuhan, 430070, China.
Hubei Maglev Engineering Technology Research Center, Wuhan, 430070, China.
Hubei Key Laboratory of Digital Manufacturing, Wuhan University of Technology, Wuhan, 430070, China.
E-mail: song.chsh@163.com*

Xin Ma

School of Mechanical and Electronic Engineering, Wuhan University of Technology, Wuhan, 430070, China.

Han Wu

Lesso-KOE Technology Industry Co. Ltd, Foshan, 523595, China.

Zhihui Mai

Keen Offshore Engineering Co. Ltd, Foshan, 528241, China.

(Received 31 August 2022; accepted 4 January 2023)

With the improvement of machining accuracy, external low frequency vibration has become one of the most important factors affecting the performance of equipment. The theory of quasi-zero stiffness vibration isolation shows favorable low frequency vibration isolation effect. However, the theory, mechanical properties and dynamics of the system still need to be studied and expanded. Based on our previous research on the structure of a magnetic-air hybrid quasi-zero stiffness vibration isolation system, the nonlinear mechanical expression of positive and negative stiffness structure has been analyzed in this paper, to improve application of the system and provide a theoretical basis for sequential studies of active control. To provide the judgment criteria and basis for the application of quasi-zero stiffness, a more accurate quasi-zero stiffness mechanical model was to be established, and the judgment criterion and stability of quasi-zero stiffness was to be discussed and analyzed. Then, the dynamical model based on external low frequency vibration was developed, to investigate the stability and natural frequency. At the same time, the influence of different feedback parameters on the amplitude frequency characteristics has been discussed, which provides a basis for the future study of active control. Finally, we carried out simulation and experimental analysis to verify the stiffness of high static and low dynamic and the low frequency vibration isolation effect of the vibration isolation system.

1. INTRODUCTION

With manufacturing equipment and processing technology advancing into nanometer, the low frequency vibration of the environment has gradually become a key factor affecting the performance and accuracy of precision instruments.^{1,2} After reviewing many literatures, we find that low frequency vibration mainly comes from the vibration and noise of seismic shudder, working environment and personnel flow. Besides, the frequency ranges from 0 Hz to 10 Hz.³⁻⁵ Therefore, to guarantee the precision performance of instrument, it is extremely necessary to suppress external low-frequency vibration interference. Because the nonlinear vibration isolation theory shows favorable low frequency vibration isolation effect, it has been researched and applied extensively in the field of low frequency vibration isolation. In particular, the theory of quasi-zero stiffness is characterized by high static stiffness and low dynamic stiffness, which has attracted more and more attention in the field of nonlinear vibration isolation.⁶⁻¹⁰

In 1957, Molyneux first proposed the concept of quasi-zero stiffness, and classified and analyzed vibration isolation structures with different negative stiffness.¹¹ R.A. Ibrahim introduced the basic concepts and inherent nonlinear phenomenon of nonlinear vibration isolator, and summarized the specific types of nonlinear vibration isolators.¹² Recently, the structure of gasbag and magnetism is one of the research focuses. Yang summarized different types of electromagnetic quasi-zero stiffness structures, and analyzed the working principles of different structures.¹³ Robertson established a 6-DOF quasi-zero stiffness structure with permanent magnet, proposed the design concept and relevant theory, and studied its mechanical structure and control system.¹⁴ To realize the stiffness characteristics of high static and low dynamic, Wang designed a quasi-zero stiffness vibration isolator in the form of Maxwell's electromagnetic force and mechanical spring in parallel, and analyzed the expression of electromagnetic force and dynamics of the system.¹⁵ Gao proposed a pneumatic near-zero frequency vibration isolator, which contained two important ele-

ments: gas and liquid. In addition, Gao established a mixed pneumatic dynamic model and verified the performance of large load and low-frequency vibration isolation.¹⁶ Chen analyzed the effective area and mechanical properties of the air suspension element structure, and analyzed the nonlinear dynamics of the quasi-zero stiffness air suspension system using the cell-mapping method.¹⁷ Salvatore analyzed the nonlinear performance from three aspects of path following, bifurcation analysis and time integration based on bistable mechanisms together with the tunable superelasticity.¹⁸ What's more, Salvatore also discussed the advantages of negative stiffness and the existence of rich bifurcation scenarios toward quasiperiodicity. Vo designed a quasi-zero stiffness structure using pneumatic cylinder with auxiliary chamber, determined and verified the pressure-change model of the air spring.¹⁹ In addition, the influence of the parameters on the nonlinear dynamics of the system was comprehensively analyzed.

To sum up, in terms of airbag and magnetic structure, its theory, mechanical properties and dynamics of quasi-zero stiffness vibration isolation system still need to be expanded and studied. Prior to this paper, we designed a magnetic-air hybrid quasi-zero stiffness vibration isolation structure, and preliminarily analyzed its mechanical properties.²⁰ Therefore, in this paper, the mathematical model of positive stiffness structure and negative stiffness structure will be further deduced to improve its applicability. A more accurate quasi-zero stiffness mechanical model is to be established. At the same time, the judgement criterion and stability of quasi-zero stiffness is to be discussed and analyzed, which provides the judgment criteria and basis for the application of quasi-zero stiffness. What's more, to provide theoretical basis for subsequent active control, the dynamic model of passive-mode and passive-active mode are analyzed, and the influence of different feedback parameters on the system is discussed. Eventually, Simulation and experimental platform of passive mode are built to investigate and verify the effect of the vibration isolation system.

2. MATHEMATICAL MODELS OF POSITIVE AND NEGATIVE STIFFNESS ELEMENT

The structure of the adjustable magnetic-air quasi-zero stiffness isolator in the early stage was shown in reference 19 (the structure was also shown in Appendix A). In the previous studies, it was assumed that when the pressure p was determined, the stiffness of air spring was constant and the static balance position was at $x = h$. As the corresponding static balance position of different equipment varied, the electromagnetic springs and universal joints need to be adjusted at the same time, thus leading to complex adjustment of the system. Therefore, this part analyzed and improved the structural mathematical model, what's more, studied the general judgement criterion of quasi-zero stiffness of the magnetic-air hybrid vibration isolation system.

2.1. Mathematical Models of Positive Stiffness Element

The air spring was a vibration isolator that can achieve bearing and vibration isolation by compressing gas. It was assumed in this paper that there was no air leakage in the air spring, namely, the volume of the air spring remained unchanged. When the volume kept constant, the greater the compression was, the larger the effective cross section would be. Therefore,

according to ideal gas equation of state and mechanical equation,²¹⁻²³ and it was assumed that there was a linear relationship between compression and effective cross section, we then obtained the stiffness equation of air spring, as was depicted in Eq. (1).

$$K_a = \frac{\partial F_a}{\partial x} = \frac{-\lambda \left(\frac{V_0}{V_1}\right)^\lambda (p_0 + p_a)}{V_1} \frac{\partial V_1}{\partial x} + \left[\left(\frac{V_0}{V_1}\right)^\lambda (p_0 + p_a) - p_a \right] \cdot \frac{\partial s_e}{\partial x};$$

$$K_a \approx \lambda (p_0 + p_a) \left[\frac{\kappa^2}{V_1} x^2 + \frac{2\lambda(p_0 + p_a)\kappa s_0}{V_1} x + \frac{\lambda(p_0 + p_a)s_0^2}{V_1} \right] + p_0 \kappa \tag{1}$$

where V_n was the volume of air spring at any time; s_e , x , s_0 and κ were effective cross section, compression, initial effective cross section and proportional coefficient of air spring, respectively; the relationship between these variables was $\begin{cases} V_n = \text{constant} \\ s_e = \kappa x + s_0 \end{cases}$ $p = \text{certain}$; p_a , p_0 and V_0 were atmospheric pressure, initial state air spring pressure and initial state volume, respectively; λ , p_1 and V_1 were polytrophic exponent, pressure and volume of air spring under current state, respectively; F_a was the air spring force when the pressure value was p_1 , the relationship between these variables was $\begin{cases} (p_1 + p_a) V_1^\lambda = (p_0 + p_a) V_0^\lambda \\ F_a = p_1 s_e \end{cases}$. The derivative of F_a with respect to x was carried out, and the stiffness theoretical Eq. (1) can be obtained.

It could be figured out from Eq. (1) that the stiffness of the air spring had a quadratic functional relationship with compression x and a proportional relationship with pressure p , namely, the force had a cubic relationship with compression x . Therefore, the stiffness of the air spring could not be simply equivalent to a constant, which could affect the static balance of the magnetic-air hybrid quasi-zero stiffness vibration isolation system.

The parameters of the air spring mathematical model could be obtained via the combination of experiment and fitting, which could be equivalently expressed as Eq. (2). The comparison between experiment and fitting of air spring was displayed in Fig. 1. It can be seen from Fig. 1 that it has a good degree of fitting, and the error relative to the experimental data is within 5%. It verified that Eq. (2) could well display the mechanical properties of air spring

$$\begin{cases} F_a = (aP + b) (cx^3 + dx^2 + ex + g) \\ K_a = (aP + b) (3cx^2 + 2dx + e) \end{cases}; \tag{2}$$

where (a, b, c, d, e) were the polynomial coefficient of air spring.

2.2. Mathematical Model of Negative Stiffness Element

To meet a different state of static balance, the mathematical expression of the electromagnetic spring was simplified to make it applicable in a certain range. Currently, the expression did not vary with the state of static balance. According to the previous studies²⁰ and the electromagnetic theory,²⁴ an

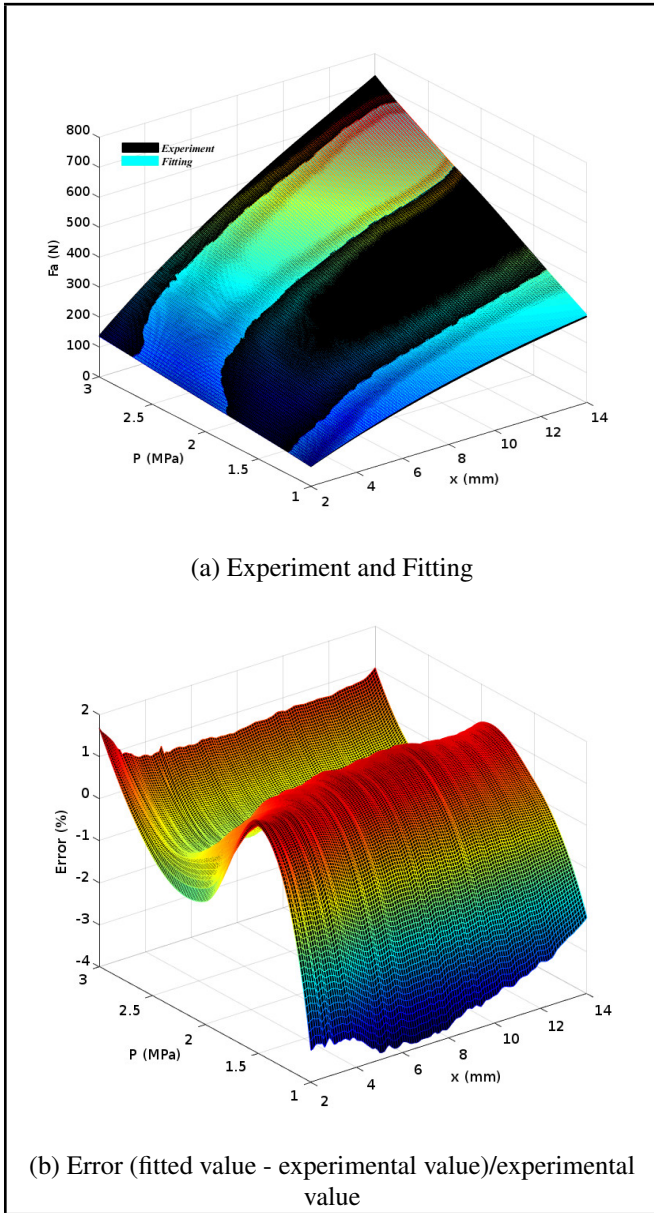


Figure 1. Comparison between experiment and fitting of air spring bearing capacity.

equation could be obtained as follows:

$$\begin{cases} F_z = 2k_s z - \frac{\mu_0 \mu_r A N^2 I^2}{4} \left(\frac{1}{(S-z)^2} - \frac{1}{(S+z)^2} \right) \\ K_z = 2k_s - \mu_0 \mu_r A N^2 I^2 S \cdot \frac{S^2 + 3z^2}{(S^2 - z^2)^3} \end{cases}; \quad (3)$$

where k_s was the mechanical spring stiffness inside the electromagnetic structure; μ_0 and μ_r were absolute permeability and relative permeability respectively; A and NI were the effective cross section and ampere-turns of the electromagnetic structure respectively; S and z were air gap and horizontal displacement of electromagnetic structure respectively. Because the state of static balance (z) was variable, it was inappropriate to adopt Taylor Expansion to simplify the Eq. (3). When $z \ll S$, from Eq. (3), the stiffness K_z approximately had a quadratic function relationship with I and z . If $z = nS$ ($0 \leq n \leq 1$), Eq. (3) could be expressed as:

$$\begin{cases} F_z = \alpha I^2 z^3 + \beta I^2 z^2 + (\gamma I^2 + \xi) z + \delta I^2 \\ K_z = 3\alpha I^2 z^2 + 2\beta I^2 z + \gamma I^2 + \xi \end{cases}; \quad (4)$$

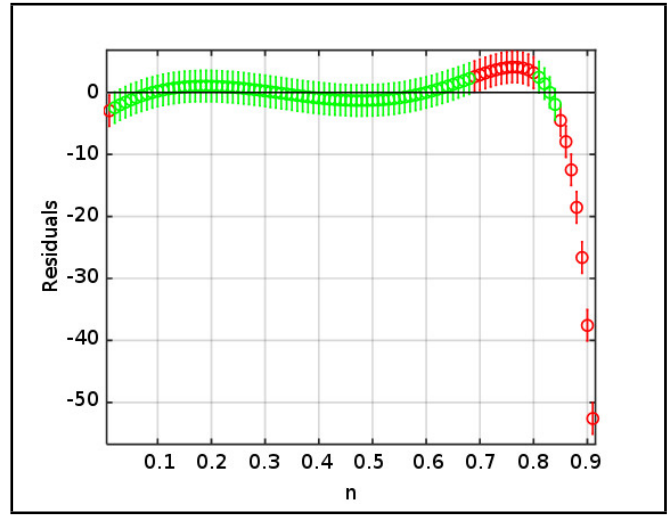


Figure 2. Residual analysis electromagnetic force.

where $(\alpha, \beta, \gamma, \xi, \delta)$ were the polynomial coefficient of negative stiffness element.

Taking the theoretical Eq. (3) as the data sample, this paper analyzed the reliability of Eq. (4) at the 95% confidence level. We imported the parameters in Appendix A into Eq. (3) to obtain the residual analysis results, as was showed in Fig. 2. Fig. 2 indicated that when $n \rightarrow 0$, the change of initial magnetic field B was excessively small, and when $n \rightarrow 0.7$, the nonlinearity of electromagnetic force was greatly strengthened. It followed that Eq. (4) was not credible because it was not within the confidence interval. Therefore, when $n \in (0.05, 0.6)$, the expression of electromagnetic force could be simplified to Eq. (4). In other words, the equation remained constant within this range.

According to Eq. (4), when the current was constant ($I = I_b$), the vibration isolation system was a passive quasi-zero stiffness isolator with variable parameters; when the current was $I = I_b + \Delta i$, the system became an active-passive mode. Since the control strategy and active control system of the active-passive mode were under research, they may not be described in depth in this paper.

3. JUDGEMENT CRITERION AND STABILITY ANALYSIS QUASI-ZERO STIFFNESS VIBRATION ISOLATION SYSTEM

3.1. Mechanical Model and Judgement Criterion

According to Eq. (2) and Eq. (4), if $y = x - h$ (Appendix A), the mechanical model of magnetic-air hybrid quasi-zero stiffness vibration isolation system could be deduced as:

$$\begin{aligned} F &= F_a + 4F_z \cdot \tan \theta \\ &= (aP + b) \left[c(y + h)^3 + d(y + h)^2 + e(y + h) + g \right] + \\ &4 \left[\left(\alpha I^2 \left(\sqrt{L^2 - y^2} - a \right)^3 + \beta I^2 \left(\sqrt{L^2 - y^2} - a \right)^2 \right. \right. \\ &\quad \left. \left. + (\gamma I^2 + \xi) \left(\sqrt{L^2 - y^2} - a \right) + \delta I^2 \right) \right] \frac{-y}{\sqrt{L^2 - y^2}}. \end{aligned} \quad (5)$$

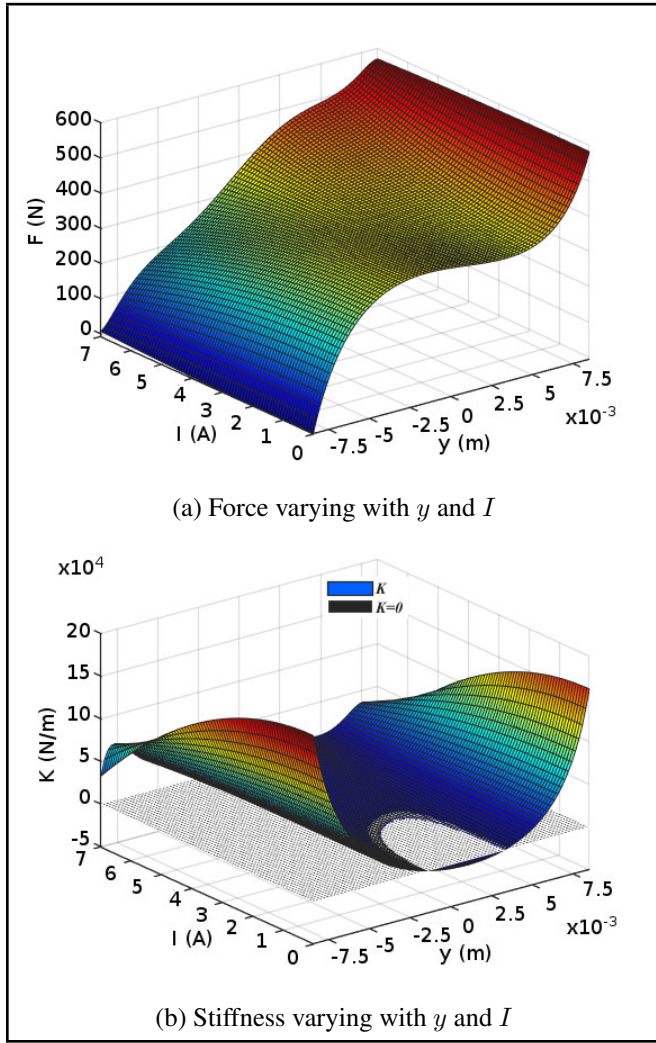


Figure 3. Force and stiffness of the system.

We input the parameters (Appendix A) into Eq. (5), then the force and the stiffness of the system were displayed in Fig. 3.

Fig. 3 showed that the current I can change the force and stiffness of the system. When the structural parameters of vibration isolation system were determined, the quasi-zero stiffness could be adjusted by changing the current I . Of course, the range of I was not infinite. Once the current I exceeded the range, the system wasn't quasi-zero stiffness. Due to the non-linear characteristic of air spring and electromagnetic spring, the static balance was not at the state of $y = 0$ ($x = h$). Therefore, $K|_{y=0} = 0$ could not be simply used as the judgement criterion of quasi-zero stiffness.

Based on the stability of the system and the theory of quasi-zero stiffness, the paper put forward the following judgement criterion of quasi-zero stiffness of the magnetic-air hybrid quasi-zero stiffness vibration isolation system:

$$\begin{aligned} &\text{When } p = \text{certain,} \\ &\exists I \text{ make } \begin{cases} \exists y, K \rightarrow 0 \text{ and } \frac{\partial K}{\partial y} = 0 \\ \forall y, K \geq 0 \end{cases} \\ &(y_{\min} \leq y \leq y_{\max}, I_{\min} \leq I \leq I_{\max}). \end{aligned} \quad (6)$$

According to the judgement criterion of Eq. (6), current I and static balance position y of quasi-zero stiffness were shown in Fig. 4.

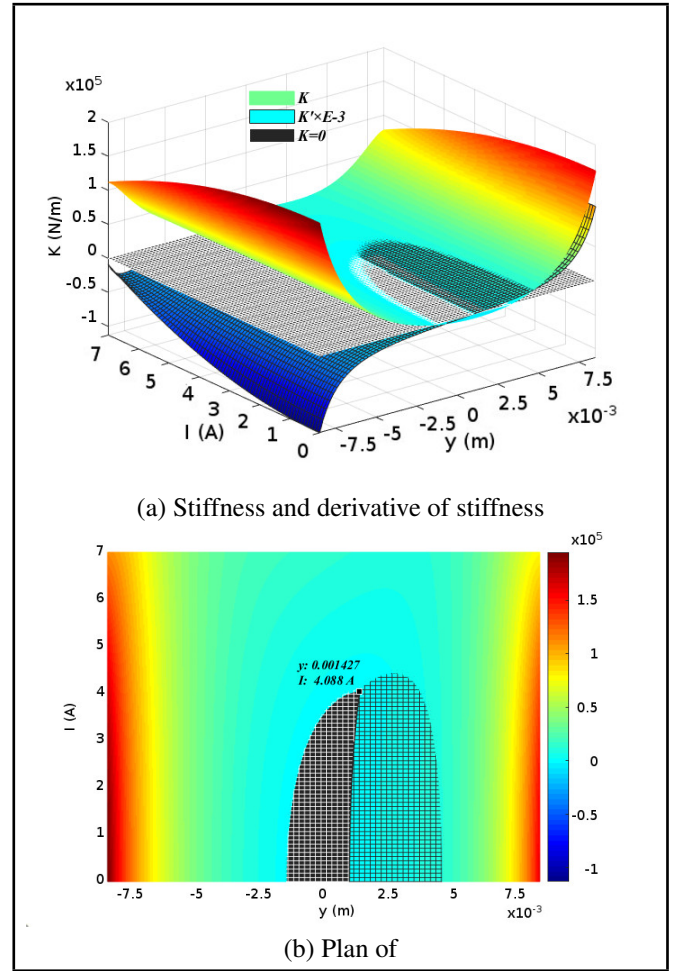


Figure 4. Change of quasi-zero stiffness with current I and static balance position y .

3.2. Stability Analysis

The analysis methods of kinematics of nonlinear system can be divided into qualitative analysis and quantitative analysis.²⁵ Among them, quantitative analysis can directly reflect the main characteristics of nonlinear system. The phase plane method, one of the most intuitive qualitative analysis methods, describes the kinematics of the system through phase trajectory.^{26,27}

In this paper, the vibration isolation system mainly isolated vibration from the ground and reduced the external interference to the equipment installed on vibration isolation system. x_j and x were the displacement signal of ground vibration and the response displacement signal of equipment, respectively. The dynamics equation of the system was as follows:

$$c(\dot{x}_j - \dot{x}) + F - mg = m\ddot{x}. \quad (7)$$

We assumed that the ground vibration interference was $x_j = A \cos(\omega t)$ and brought it into Eq. (7). The phase trajectory in the coordinate plane of $x - \dot{x}$ was then obtained. The phase trajectory at $\omega = (2\text{Hz}, 3\text{Hz}, 4\text{Hz}, 5\text{Hz}, 6\text{Hz}, 7\text{Hz}, 8\text{Hz}, 9\text{Hz})$ was displayed in Fig. 5, where the blue line represented the displacement and velocity of the external excitation, and the red line represented the displacement and velocity of the response of the quasi-zero stiffness isolation system.

According to the displacement and velocity of external excitation and system response in the phase trajectory, if the displacement and velocity of the system response are oscillatory,

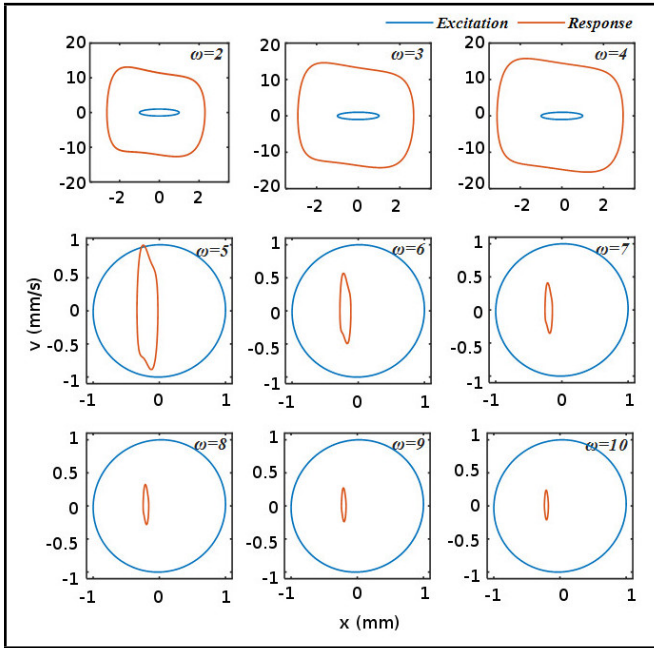


Figure 5. Phase trajectory of magnetic-air hybrid quasi-zero stiffness vibration isolation system.

the system was considered to be in stability (asymptotic stability). the circle size of the red line and blue line was used to judge whether the amplitude of the system response is less than the excitation amplitude. If the size of red is smaller than the size of blue, we thought that the system has vibration isolation effect at this frequency. From the phase trajectory under different frequency displacement interference, it could be figured out that the vibration isolation system showed good stability. The comparative analysis between interference signal and response signal indicated that when the frequency of external interference signal was 5 Hz ($\omega = 5\text{Hz}$), the system had favorable vibration isolation effect in terms of the displacement signal; while vibration isolation effect couldn't be found in terms of the velocity signal. This suggested that the natural frequency of the magnetic-air hybrid quasi-zero stiffness vibration isolation system was about 4 Hz. The phase trajectory not only verified the stability of the system, but also indirectly demonstrated the low dynamic stiffness of the vibration isolation system.

4. DYNAMICS AND INFLUENCE OF CONTROL PARAMETERS

4.1. Dynamics Analysis of Passive Mode

Based on Eq. (7), the dynamic equation from the ground to the equipment was established to analyze the favorable effect of the vibration isolation system on external interference. According to the above equations, the pressure p and current I didn't change with time, the system was passive and the force of the system was a cubic function of the compression y . At the same time, the mass supported by the system had nothing to do with dynamic stiffness, but was related to the initial height of air spring. Therefore, we assumed that, when the system approached static balance, the force expression of the system was approximately defined as $F = k\Delta x^3 + mg$.

Assuming $\mu = x - x_j$ and $x_j = X_j \cos(\omega t)$, the dynamic differential equation of passive mode was expressed as:

$$\ddot{\mu} + \frac{c}{m}\dot{\mu} - \frac{k}{m}(-\mu)^3 = \omega^2 X_j \cos(\omega t). \quad (8)$$

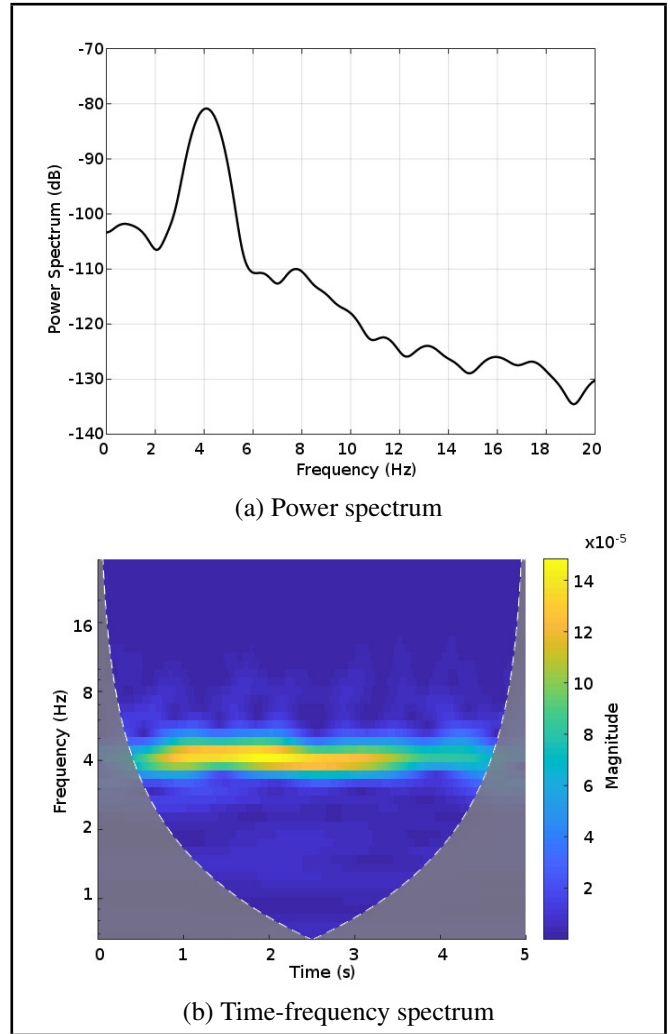


Figure 6. The power spectrum and time-frequency spectrum.

According to the theory of harmonic balance method, if $\mu = A \sin(\omega t + \varphi)$, Eq. (8) could be equivalent to:

$$-\omega^2 A \sin(\omega t + \varphi) + \frac{c}{m} \omega A \cos(\omega t + \varphi) - \frac{k}{m} (-A \sin(\omega t + \varphi))^3 = \omega^2 X_j \cos(\omega t). \quad (9)$$

By solving dynamic equations, the amplitude frequency characteristic and phase frequency characteristic could be obtained:

$$\begin{cases} (\omega^2 X_j)^2 = \left(\omega^2 A - \frac{3kA^3}{4m} \right)^2 + \left(\frac{c\omega A}{m} \right)^2 \\ \tan \varphi = \frac{-\omega m}{c} + \frac{3kA^2}{4c\omega} \end{cases}. \quad (10)$$

On the basis of mathematical theory, when the two roots were equal, the quadratic function took the maximum value. Thus, when $\omega_1 = \omega_2$, the displacement amplitude A reached the maximum value A_{\max} , and the expression was shown in Eq. (11):

$$A_{\max} = \sqrt{\frac{c^4}{3kmc^2 - \frac{9}{4}k^2m^2X_j^2}}. \quad (11)$$

Eq. (11) indicated that the denominator approached zero, namely, $3kmc^2 - \frac{9}{4}k^2m^2X_j^2 \rightarrow 0$. If the denominator approached zero, the maximum displacement amplitude A_{\max} approached infinity. In other words, in the resonance region,

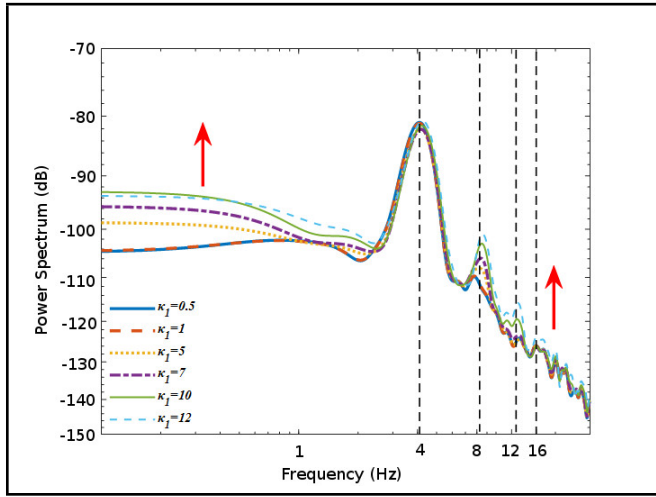


Figure 7. Influence of κ_1 on system response.

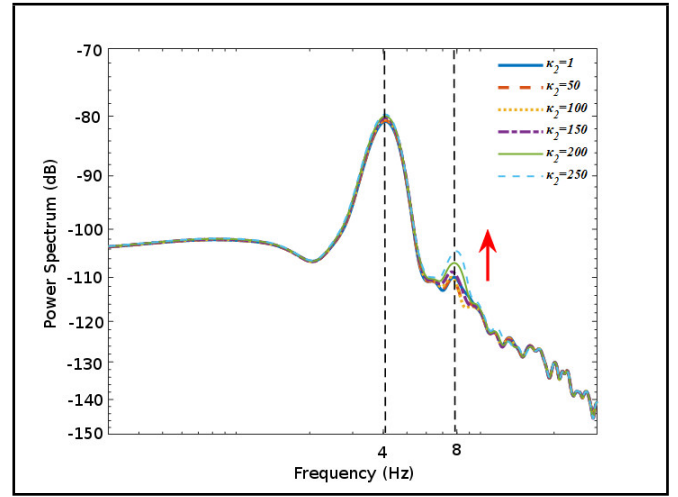


Figure 8. Influence of κ_2 on system response.

the displacement response of the system was an infinity. Therefore, to achieve better performance, the following requirements shall be met:

$$3kmc^2 - \frac{9}{4}k^2m^2X_j^2 > 0 \Rightarrow 4c^2 > 3kmX_j^2. \quad (12)$$

The dynamic model of passive mode was established by using *Matlab/Simulinks*. The white noise signal of the base was used as the input and the response displacement as the output. The power spectrum and time-frequency spectrum were shown in Fig. 6.

As could be seen from Fig. 6, the resonance peak was about 4 Hz and the energy was concentrated near 4 Hz. Therefore, the natural frequency of passive mode was 4 Hz, which verified the previous conclusion.

4.2. Influence of Control Parameters on Frequency Response

When the current of electromagnetic spring was $I = I_b + \Delta i$, the system became an active-passive mode. It was assumed that the control force based on Δi of the feedback signal on the system was $\Delta F_i = \kappa_1 \Delta \ddot{x} + \kappa_2 \dot{x} + \kappa_3 x$. The force of active-passive mode was defined as $F = k\Delta x^3 + \Delta F_i + mg$. In the active-passive case, the dynamics equation of the system is as follows:

$$-\omega^2 A(m + \kappa_1) \sin(\omega t + \varphi) + \omega A(c + \kappa_2) \cos(\omega t + \varphi) + kA \sin^3(\omega t + \varphi) + \kappa_3 A \sin(\omega t + \varphi) = \omega^2 X_j \cos(\omega t); \quad (13)$$

wherein, κ_1 , κ_2 and κ_3 were the coefficient of acceleration feedback signal, the coefficient of velocity feedback signal and the coefficient of displacement feedback signal, respectively.

By solving dynamic equations, the amplitude frequency characteristic and phase frequency characteristic could be obtained:

$$\begin{cases} (m\omega^2 X_j)^2 = \left(\omega^2 A(m + \kappa_1) - \frac{3kA^3}{4} - \kappa_3 A \right)^2 + (\omega A(c + \kappa_2))^2 \\ \tan \varphi = \frac{\omega^2 A(m + \kappa_1) - \frac{3kA^3}{4} - \kappa_3 A}{\omega A(c + \kappa_2)} \end{cases} \quad (14)$$

According to Eq. (14), in addition to structural parameters, feedback control parameters were also one of one of the core

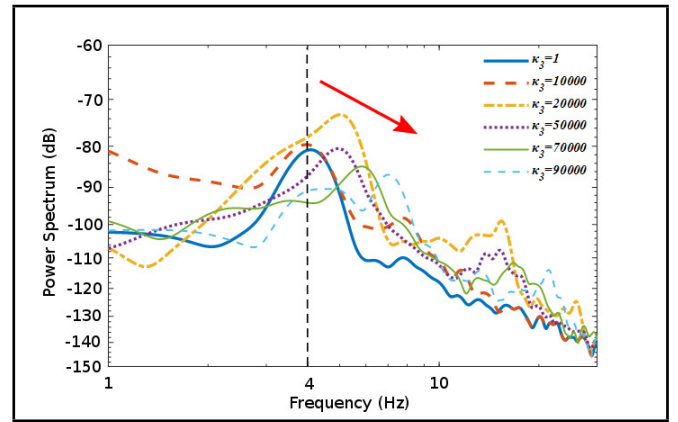


Figure 9. Influence of κ_3 on system response.

factors of the system. In this part, we analyzed the influence of different feedback parameters on the system by using the control variable method, so as to provide the basis for in-depth research on control.

One parameter was variable and the other parameter was constant (value=0). The effects of displacement, velocity and acceleration feedback gain on the system performance were analyzed. The results were shown in Figs. 7-9.

It could be figured out from the results that the acceleration feedback gain κ_1 affected whole frequency band. Because the acceleration reflects the external energy, the overall amplitude frequency curve had a certain upward shift, but it had no obvious effect on the first-order resonance. It wasn't obvious to influence of velocity feedback gain κ_2 on the whole frequency band, but it was directly proportional to the second-order resonance. The frequency of resonance was mainly affected by the displacement feedback gain κ_3 , which moved to high frequency with the increase of κ_3 , as shown by the red line in Fig. 9. To sum up, different feedback signals had different effects on the system.

5. SIMULATION AND EXPERIMENT

Since the active control strategy has under research, this part mainly carried out simulation and experimental analysis of the passive model ($I = I_b$) to verify the stability and vibration isolation effect of the passive mode.

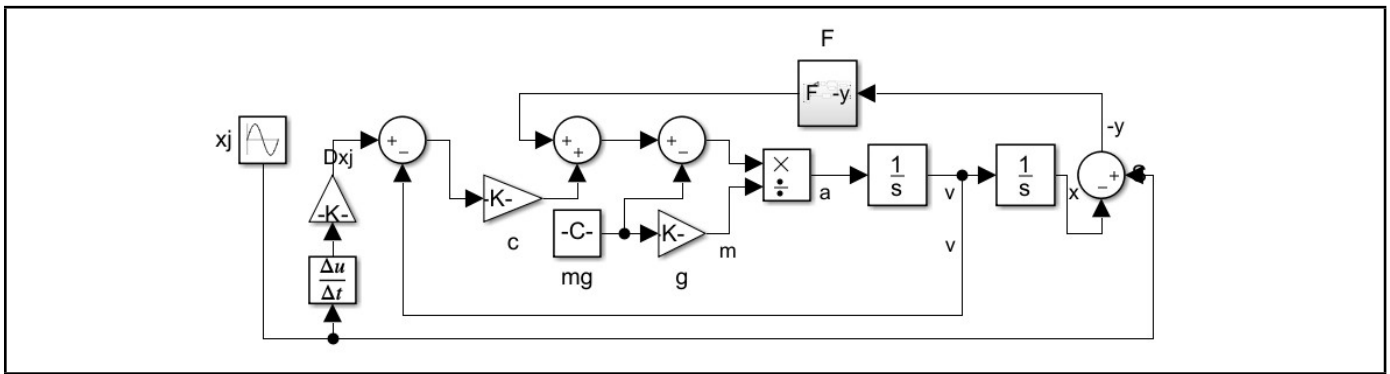


Figure 10. Simulation diagram of passive model.

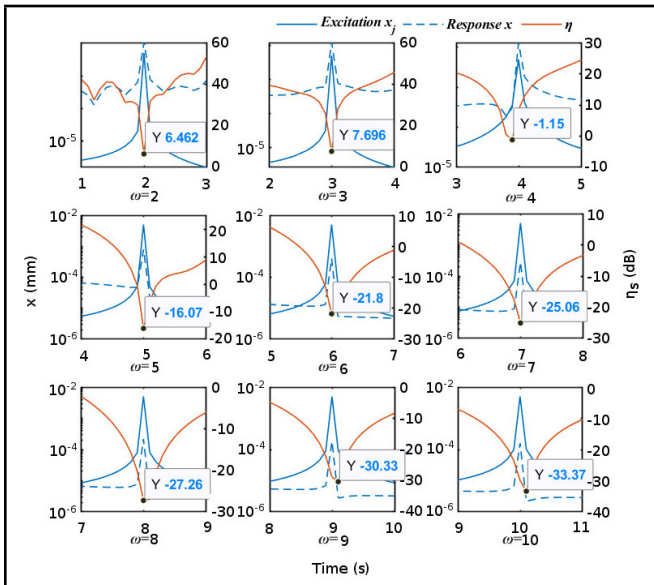


Figure 11. Simulation results of displacement transfer rate.

5.1. Simulation Analysis

According to the dynamical model of the passive system, the simulation model was developed. We chose sinusoidal displacement excitation applied on the base as the simulation interference. Because the displacement transfer rate could directly reflect the vibration reduction effect, this paper took it as an indicator.²⁸ The displacement transfer rate was the ratio of the displacement amplitude of the system response to the amplitude of the excitation, which was generally taken as $20\log$. The amplitude of sinusoidal displacement excitation in this paper was 5 mm and the simulation step was 0.001 s . The simulation diagram was displayed in Fig. 10.

The displacement transfer rate between the response signal of the equipment and the excitation signal of the base was analyzed when $\omega = (2\text{Hz}, 3\text{Hz}, 4\text{Hz}, 5\text{Hz}, 6\text{Hz}, 7\text{Hz}, 8\text{Hz}, 9\text{Hz}, 10\text{Hz})$. The simulation results were as follows Fig. 11.

The simulation results revealed that the magnetic-air hybrid quasi-zero stiffness vibration isolation system had good effect of vibration isolation from $\omega = 5\text{Hz}$. Therefore, we verified the natural frequency of the vibration isolation system was about 4 Hz . The displacement transfer rates η between 5 Hz and 10 Hz (interval 1 Hz) were respectively -16.07 dB , -21.8 dB , -25.06 dB , -27.26 dB , -30.33 dB and -33.37 dB , which suggested that the system had good effect of low frequency vibration isolation and could effectively resist external low frequency interference.

Table 1. Transfer rate.

	13.5Kg	16Kg	21Kg	5Hz	7Hz	10Hz
η	-10.29dB	-6.41dB	-5.73dB	-7.09dB	-9.29dB	-15.27dB

5.2. Experimental Analysis

We built a magnetic-air hybrid quasi-zero stiffness vibration isolation platform, as was shown in Fig. 12. Due to the limitation of experimental conditions, the acceleration signal was collected to analyze the effect of vibration isolation.

Based on the experimental platform, two groups of experiments were carried out. One group was aimed to analyze different vibration isolated objects. We chose 13.5 kg , 16 kg and 21 kg respectively as the mass of equipment. In addition, the excitation signal was the sinusoidal signal with frequency of 5 Hz generated by the actuator. The experimental results were shown in Figs 13-15. The other group was designed to investigate the effect of vibration isolation under different low frequency interference. The external interference was sinusoidal excitation with frequency of 5 Hz , 7 Hz and 10 Hz . Additionally, the mass was a fixed value and the pressure of air spring was 0.1 MPa . Figs. 16-17 showed the experimental results. The transfer rate of all experiments was displayed in Table 1.

According to Figs. 13-15 and Table 1, when the mass was 13.5 kg , 16 kg and 21 kg , respectively, the vibration isolation effects are, respectively, 10.29 dB , 6.41 dB and 5.72 dB . With the increase of mass, its vibration isolation effect was worse. This was because the heavier the load was, the larger the positive stiffness proportion of the air spring in the system was, and the quasi-zero stiffness of the passive mode was gradually weakened. Therefore, the negative stiffness was changed by adjusting the current I , so that the system was as close to the quasi-zero stiffness as possible under different loads. The current regulation belonged to the active control stage, which was still studying. Although the vibration isolation effect was not consistent, it was still verified that the magnetic-air hybrid vibration isolation system showed high static stiffness and good effect of low frequency vibration isolation within a certain range of the load. In short, the magnetic-air hybrid quasi-zero stiffness system could adapt to equipment of different mass.

Based on Figs. 16–18 and Table 1, when the frequency of external excitation was 5 Hz , 7 Hz and 10 Hz , respectively, the vibration isolation effect could respectively reach 7.09 dB , 9.29 dB and 15.27 dB . Experiments indicated that the natural frequency of the vibration isolation system was lower than 5 Hz . Because the actual equipment has certain processing error, the experimental results didn't directly verify that the natural frequency was about 4Hz , but 5Hz was about 4Hz which indirectly proves the validity of the theory. With the increase of

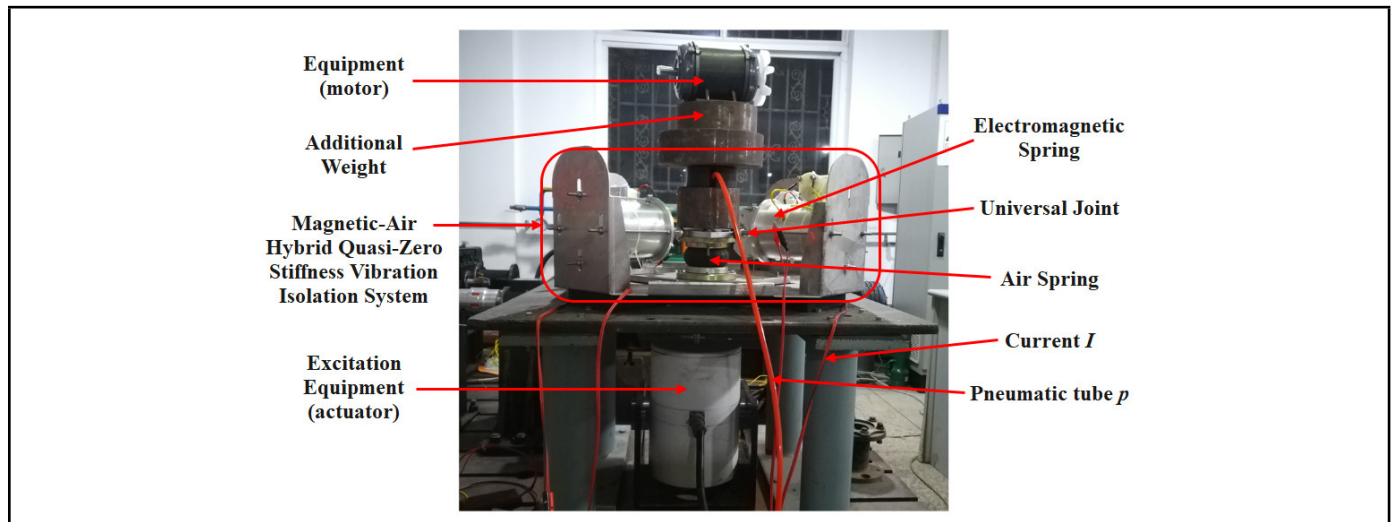


Figure 12. Experimental platform.

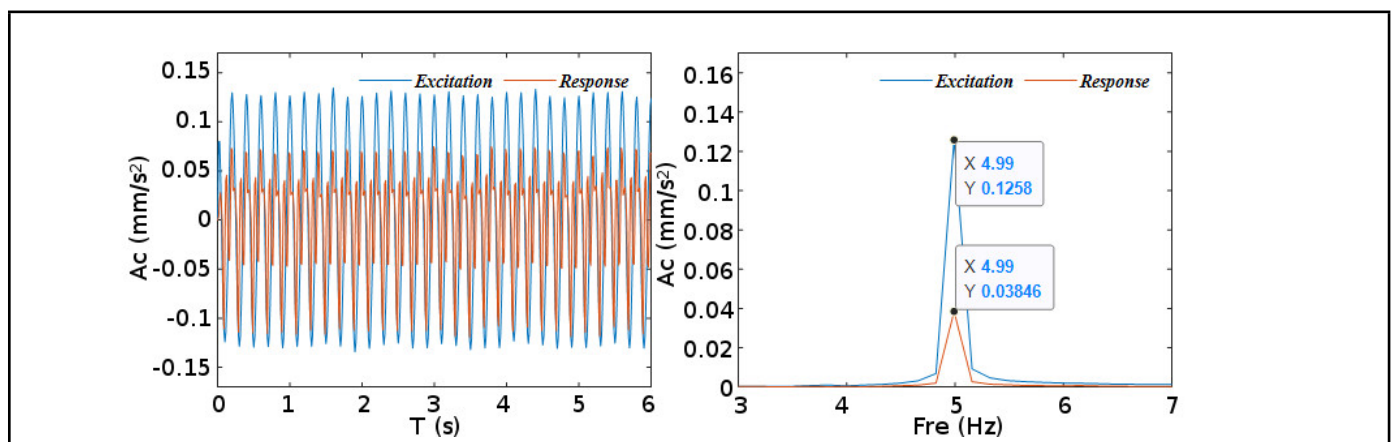


Figure 13. Experimental results of vibration isolation with mass of 13.5kg.

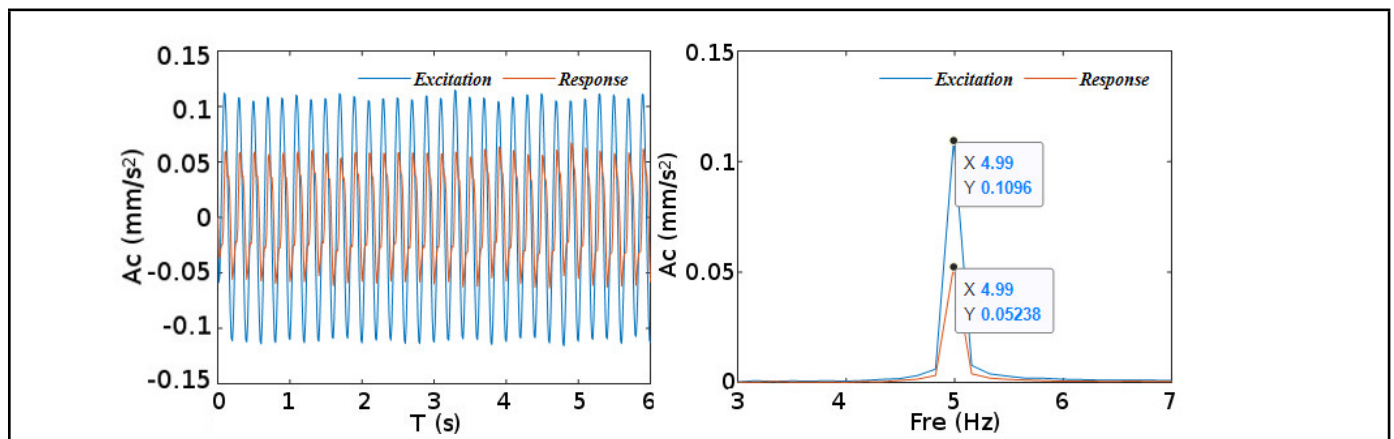


Figure 14. Experimental results of vibration isolation with mass of 16kg.

frequency, the vibration isolation effect became better and better, which was because the frequency of external interference is greater than $\sqrt{2}$ times the natural frequency. To sum up, in a certain low frequency vibration range, the magnetic-air hybrid quasi-zero stiffness system had a good low frequency vibration isolation effect.

6. CONCLUSION

Based on our previous research on the structure of magnetic-air hybrid quasi-zero stiffness vibration isolation system, the

mathematical model expression of positive and negative stiffness elements has been further analyzed to improve the application of the mathematical model. The mathematical model of vibration isolation system has been established, and the judgement criterion of magnetic-air hybrid quasi-zero stiffness has been analyzed. It has been figured out that the static balance was not at $y = 0$ ($x = h$). In this paper, external interference was considered as excitation signal, while vibration of the equipment as response signal. Employing the phase trajectory method, we have validated the stability of the vibra-

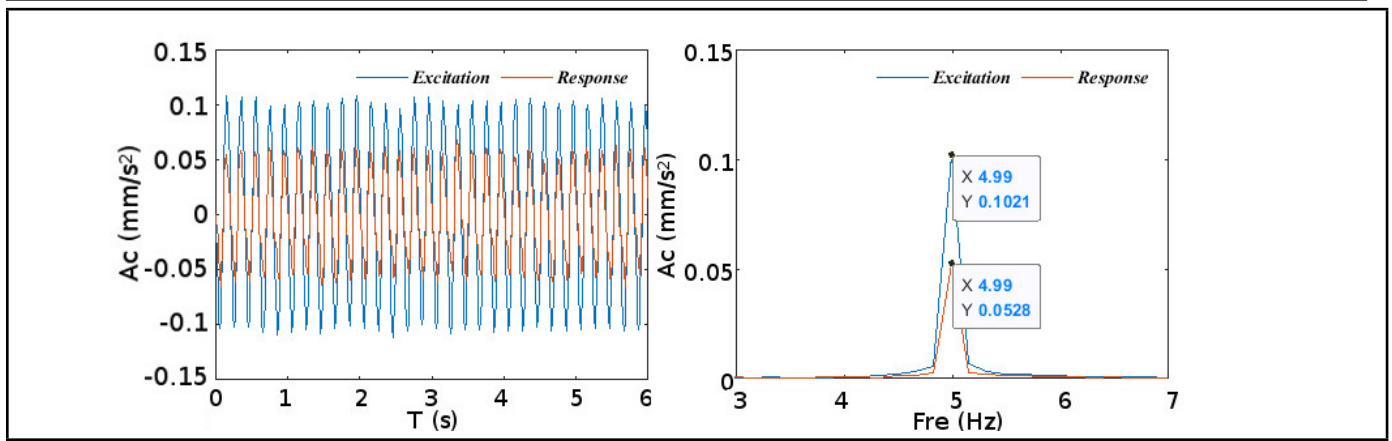


Figure 15. Experimental results of vibration isolation with mass of 21kg.

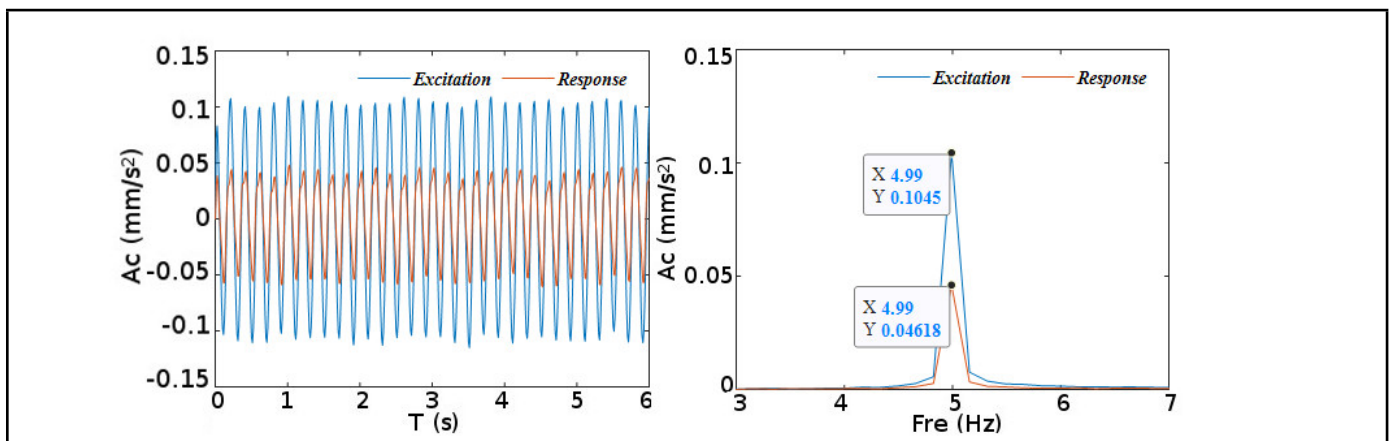


Figure 16. Experimental results of vibration isolation when $w = 5\text{Hz}$.

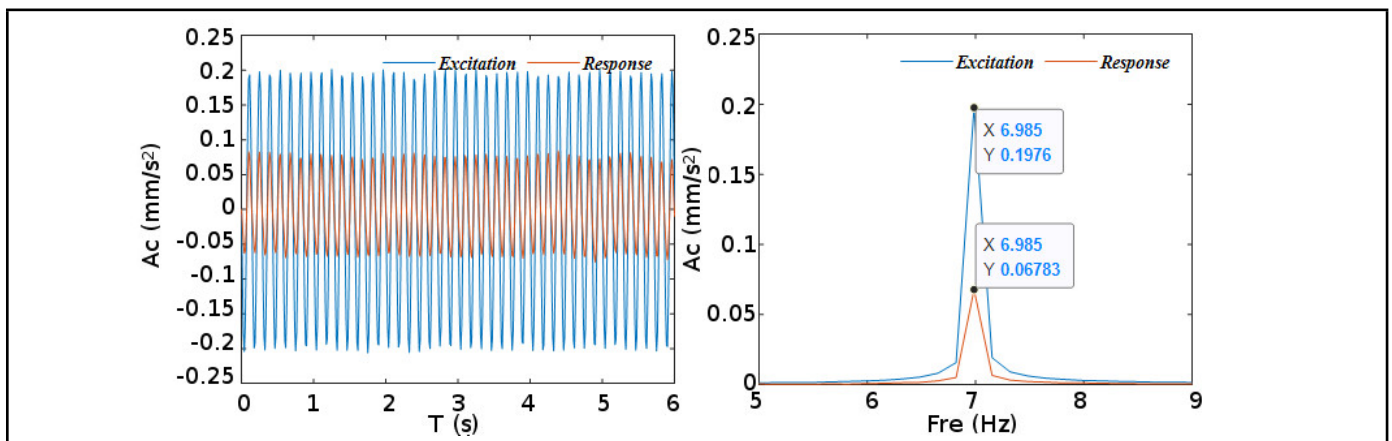


Figure 17. Experimental results of vibration isolation when $w = 7\text{Hz}$.

tion isolation system and that the natural frequency of the system was within 4Hz. What's more, this paper has built the dynamics, and analyzed the influence of active control feedback on the system. It found out that the coefficient of acceleration feedback signal affected whole frequency band; the second-order resonance was proportional to the coefficient of the velocity feedback signal. It provided a certain basis for the selection of feedback parameters. Additionally, the low frequency vibration isolation effect of the vibration isolation system has been simulated and tested. The results indicated that the magnetic-air hybrid quasi-zero stiffness vibration isolation system could adapt to different equipment whose mass was in a certain range. Meanwhile, for different external low

frequency interference, the system could achieve vibration isolation effect of more than 7 dB.

DATA AVAILABILITY

The data used to support the findings of this study have been included within the article.

ACKNOWLEDGEMENTS

This work was supported by the National Natural Science Foundation of China (No. 51879209) and the Fundamental Research Fund for the Central Universities (China, No. 2020-YB-026, No. WUT: 2021IVA117).

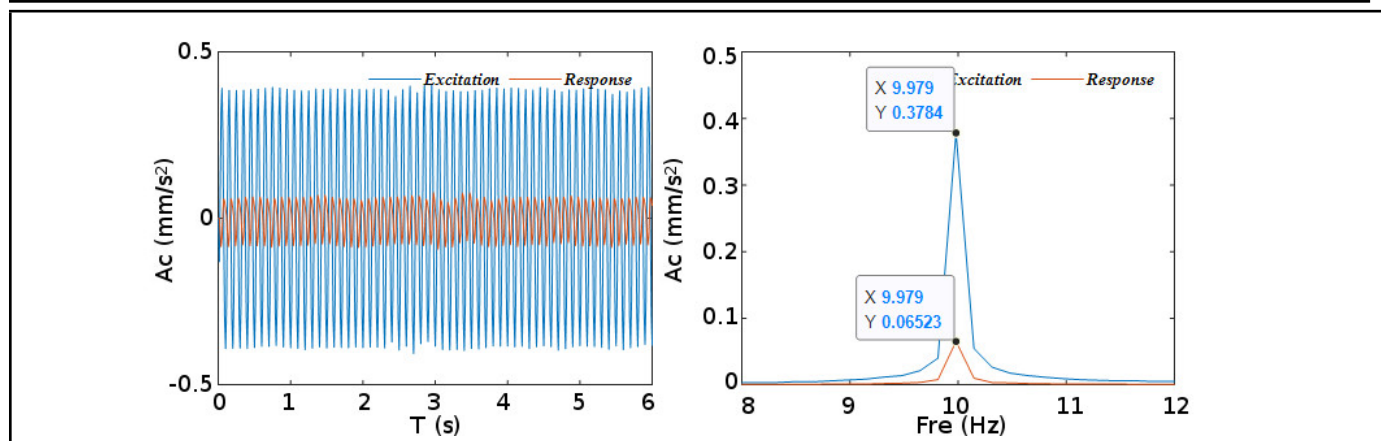


Figure 18. Experimental results of vibration isolation when $w = 10\text{Hz}$.

COMPETING INTERESTS

The authors declare that there are no conflicts of interest regarding the publication of this paper.

REFERENCES

- ¹ Balaji, P. S. and K. Karthik SelvaKumar. Applications of Nonlinearity in Passive Vibration Control: A Review, *Journal of Vibration Engineering & Technologies*, 1-31, (2020). <https://doi.org/10.1007/s42417-020-00216-3>
- ² Chang L. Micro electromechanical systems (MEMS): technology and future applications in circuits, *International Conference on Solid-state & Integrated Circuit Technology IEEE*, (1998). <https://doi.org/10.1109/ICSICT.1998.786526>
- ³ Iii J., Skelton D. Department of Defense need for a micro-electromechanical systems (MEMS) reliability assessment program, *Proceedings of SPIE-The International Society for Optical Engineering*, (2005). <https://doi.org/10.1117/12.602257>
- ⁴ Hassan M., Dubay R., Li C. and Wang R. Active vibration control of a flexible one-link manipulator using a multivariable predictive controller, *Mechatronics*, **17**(1)(6):311-323, (2007). <https://doi.org/10.1016/j.mechatronics.2007.02.004>
- ⁵ Rademakers N. Modelling, identification and multivariable control of an active vibration isolation system, *Masters Thesis*. (2005).
- ⁶ Ibrahim R.A. and Pettit C.L. Uncertainties and dynamic problems of bolted joints and other fasteners, *Journal of Sound and Vibration*, **279**(3-5):857-936, (2005). <https://doi.org/10.1016/j.jsv.2003.11.064>
- ⁷ G. Takács and B. Rohal'-Ilkiv. Smart Materials in Active Vibration Control, *Springer London*, (2012). <https://doi.org/10.1007/978-1-4471-2333-0>
- ⁸ Ma Z.Z., Zhou R.P. and Yang Q.C. Recent Advances in Quasi-Zero Stiffness Vibration Isolation Systems: An Overview and Future Possibilities, *Machines*, **10**(9):813, (2022). <https://doi.org/10.3390/machines10090813>
- ⁹ C. Liu, X. Jiang, Steve Daley and Fengming Li. Recent advances in micro-vibration isolation, *Mechanical Systems and Signal Processing*, **56/57**:55-80, (2015). <https://doi.org/10.1016/j.ymssp.2014.10.007>
- ¹⁰ Zotov A. and Valeev A. Vibration Isolating and Impact Protecting Systems with Quasi-Zero Stiffness Providing Wide Operating Area, *Springer*, (2020). https://doi.org/10.1007/978-3-030-22041-9_34
- ¹¹ Molyneux W. Supports for vibration isolation, *Great Britain: Aeronautical Research Council*, (1957).
- ¹² Ibrahim R.A. Recent advances in nonlinear passive vibration isolators, *Journal of Sound and Vibration*, **314**(3): 371-452, (2008). <https://doi.org/10.1016/j.jsv.2008.01.014>
- ¹³ Yan B., Yu N. and Wu C.Y. A state-of-the-art review on low-frequency nonlinear vibration isolation with electromagnetic mechanisms, *Applied mathematics and mechanics-English edition*, **43**(7): 1045-1062, (2022). <https://doi.org/10.1007/s10483-022-2868-5>
- ¹⁴ Zhu T., Cazzolato B., Robertson W.S.P. and Zander A. Vibration isolation using six degree-of-freedom quasi-zero stiffness magnetic levitation, *Journal of Sound and Vibration*, **358**: S0022460X15005866, (2015). <https://doi.org/10.1016/j.jsv.2015.07.013>
- ¹⁵ Wang M.T., Su P., Liu S.Y., Chai K., Wang B.X. and Lu J.F. Design and Analysis of Electromagnetic Quasi-zero Stiffness Vibration Isolator, *Journal of vibration engineering & Technologies*, (2022). <https://doi.org/10.1007/s42417-022-00569-x>
- ¹⁶ Gao X., Teng H.D. Dynamics and isolation properties for a pneumatic near-zero frequency vibration isolator with nonlinear stiffness and damping, *Nonlinear dynamics*, **102**(4): 2205-2227, (2020). <https://doi.org/10.1007/s11071-020-06063-x>
- ¹⁷ Chen L., Wang J., Xu X., et al. Nonlinear Analysis of a Quasi-Zero Stiffness Air Suspension Based on the Cell-Mapping Method, *International journal of acoustics and vibration*, **26**(2): 148-160, (2021). <https://doi.org/10.20855/ijav.2021.26.21755>
- ¹⁸ Salvatore A., Carboni B. and Lacarbonara W. Nonlinear dynamic response of an isolation system with superelastic hysteresis and negative stiffness, *Nonlinear dynamics*, **107**: 1765-1790, (2022). <https://doi.org/10.1007/s11071-021-06666-y>
- ¹⁹ Vo N.Y.P., Le T.D. Static Analysis of Low Frequency Isolation Model Using Pneumatic Cylinder with Aux-

Table A.2. Basic parameters.

Structural parameters					
L	h	a			
11.404 mm	8.5 mm	7.6026 mm			
Parameters of 086060H-1 air spring					
Minimum compression	Safe elongation	Stroke Length			
44 mm	90 mm	46 mm			
Electromagnetic parameters					
μ_0	μ_r	S	A	N	I_{max}
$4\pi \times 10^{-7}$	1	10	1070.105	400	7
Vs/Am	(Vs/Am)	mm	mm ²	Turns	A

iliary Chamber, *International Journal of Precision Engineering and Manufacturing*, **21**: 681-697, (2020). <https://doi.org/10.1007/s12541-019-00301-y>

- ²⁰ Jiang Y.L., Song C.S., Ding C.M. and Xu B.H. Design of magnetic-air hybrid quasi-zero stiffness vibration isolation system, *Journal of Sound and Vibration*, **477**, (2020). <https://doi.org/10.1016/j.jsv.2020.115346>
- ²¹ Ea V., Flamm M., Steinweger T. and Weltin U. On the lifetime prediction of rolling lobe air springs, *Engineering Failure Analysis*, **94**:313-326, (2018). <https://doi.org/10.1016/j.engfailanal.2018.08.001>
- ²² Liu D.F., Jun X.U., Chen J.J. Research on the vertical stiffness characteristics of air springs based on FEA, *Manufacturing Automation*, (2011).
- ²³ Li X., Li T. Research on vertical stiffness of belted air springs, *Vehicle System Dynamics*, **51**(11):1655-1673, (2013). <https://doi.org/10.1080/00423114.2013.819984>
- ²⁴ Schweitzer G., Maslen E.H. *Magnetic Bearings-Theory, Design, and Application to Rotating Machinery, Germany*, (2009). <https://doi.org/10.1007/978-3-642-00497-1>
- ²⁵ Pascoe N. *Shock and Vibration-Theory and Practice*, John Wiley & Sons, Ltd, (2011). <https://doi.org/10.1002/9780470980101.ch5>
- ²⁶ Zhang X.H., Cao Q.J., Huang W.H. Dynamic Analysis of a Multiple-Span Euler-Bernoulli Beam Supported by Pneumatic Quasi-zero-stiffness System, *Journal of vibration engineering & technologies*, **10**:1349-1367, (2022). <https://doi.org/10.1007/s42417-022-00451-w>
- ²⁷ Conneely K., Connolly C. Vibration isolation theory and practice, *Assembly Automation*, **29**(1):8-13, (2009). <https://doi.org/10.1108/01445150910929802>
- ²⁸ Cheng C., Li S., Yong W. and Jiang X.X. Force and displacement transmissibility of a quasi-zero stiffness vibration isolator with geometric nonlinear damping, *Nonlinear Dynamics*, **87**(4):1-13, (2017). <https://doi.org/10.1007/s11071-016-3188-0>

A. APPENDIX

The structure of the adjustable magnetic-air quasi-zero stiffness isolator in the early stage was shown in Fig. A.19. The content has been published in literature 19. An air spring installed vertically was used as the positive stiffness element while four electromagnetic springs installed horizontally as the negative stiffness element. The two were connected in parallel by universal joints. The mechanical model was displayed in Fig. A.20, and the corresponding basic parameters were shown in Tab. A.2.

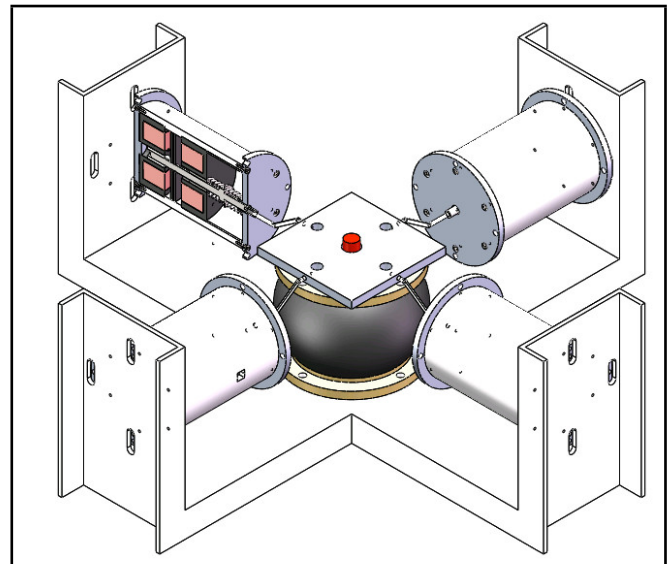


Figure A.19. Structure of magnetic-air hybrid quasi-zero stiffness vibration isolator.

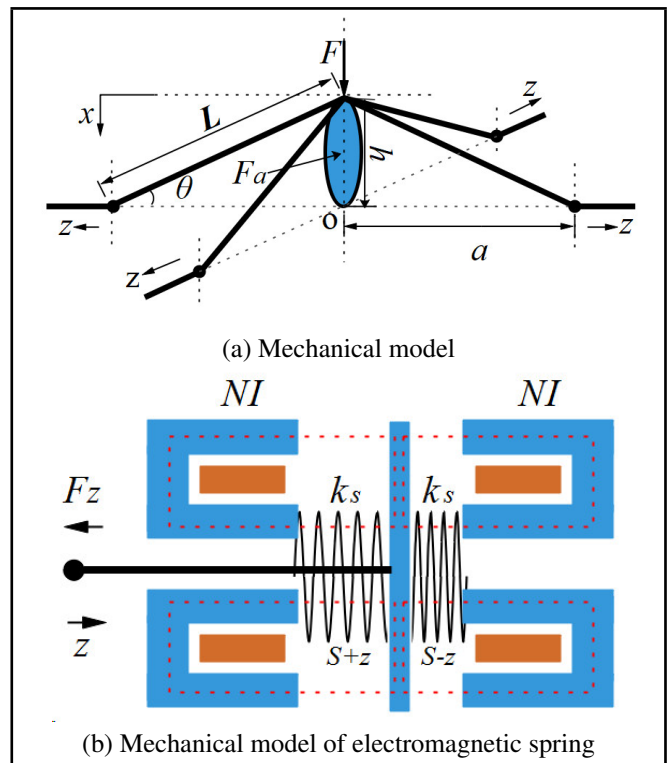


Figure A.20. Mechanical model of magnetic air hybrid quasi-zero stiffness vibration isolation system.

Table A.3. Basic parameters.

Structural parameters					
L	h	a			
11.404 mm	8.5 mm	7.6026 mm			
Parameters of 086060H-1 air spring					
Minimum compression	Safe elongation	Stroke Length			
44 mm	90 mm	46 mm			
Electromagnetic parameters					
μ_0	μ_r	S	A	N	I_{max}
$4\pi \times 10^{-7}$	1	10	1070.105	400	7
Vs/Am	Vs/Am	mm	mm ²	Turns	A